University of Groningen

Corrigendum: Short-lived positron emitters in beam-on PET imaging during proton therapy (2015 Phys. Med. Biol. 60 8923)

Dendooven, P.; Buitenhuis, H. J. T.; Diblen, F.; Heeres, P. N.; Biegun, A. K.; Fiedler, F.; van Goethem, M-J; van der Graaf, E. R.; Brandenburg, S.

Published in:
Physics in Medicine and Biology

DOI:
10.1088/1361-6560/ab23d7

IMPORTANT NOTE: You are advised to consult the publisher's version (publisher's PDF) if you wish to cite from it. Please check the document version below.

Document Version
Publisher's PDF, also known as Version of record

Publication date:
2019

Link to publication in University of Groningen/UMCG research database

Citation for published version (APA):
Dendooven, P., Buitenhuis, H. J. T., Diblen, F., Heeres, P. N., Biegun, A. K., Fiedler, F., van Goethem, M-J., van der Graaf, E. R., & Brandenburg, S. (2019). Corrigendum: Short-lived positron emitters in beam-on PET imaging during proton therapy (2015 Phys. Med. Biol. 60 8923). *Physics in Medicine and Biology*, *64*(12), [129501]. https://doi.org/10.1088/1361-6560/ab23d7

Copyright
Other than for strictly personal use, it is not permitted to download or to forward/distribute the text or part of it without the consent of the author(s) and/or copyright holder(s), unless the work is under an open content license (like Creative Commons).

The publication may also be distributed here under the terms of Article 25fa of the Dutch Copyright Act, indicated by the “Taverne” license. More information can be found on the University of Groningen website: https://www.rug.nl/library/open-access/self-archiving-pure/taverne-amendment.

Take-down policy
If you believe that this document breaches copyright please contact us providing details, and we will remove access to the work immediately and investigate your claim.

Downloaded from the University of Groningen/UMCG research database (Pure): http://www.rug.nl/research/portal. For technical reasons the number of authors shown on this cover page is limited to 10 maximum.

Physics in Medicine & Biology

IPEM Institute of Physics and Engineering in Medicine

CORRIGENDUM

Corrigendum: Short-lived positron emitters in beam-on PET imaging during proton therapy (2015 *Phys. Med. Biol.* 60 8923)

To cite this article: P Dendooven *et al* 2019 *Phys. Med. Biol.* **64** 129501

View the article online for updates and enhancements.

Recent citations

- Use of short-lived positron emitters for in-beam and real-time + range monitoring in proton therapy
A. Bongrand *et al*

- The production of positron emitters with millisecond half-life during helium beam radiotherapy
Ikechi Ozoemelam *et al*

- Offline imaging of positron emitters induced by therapeutic helium, carbon and oxygen ion beams with a full-ring PET/CT scanner: experiments in reference targets
J Bauer *et al*

This content was downloaded from IP address 129.125.148.109 on 20/01/2020 at 08:26

IOP Publishing Phys. Med. Biol. 64 (2019) 129501 (6pp) https://doi.org/10.1088/1361-6560/ab23d7

Physics in Medicine & Biology

IPEM Institute of Physics and Engineering in Medicine

CORRIGENDUM

Corrigendum: Short-lived positron emitters in beam-on PET imaging during proton therapy (2015 *Phys. Med. Biol.* 60 8923)

P Dendooven[1,5], H J T Buitenhuis[1], F Diblen[1,3], P N Heeres[1], A K Biegun[1], F Fiedler[4], M-J van Goethem[2], E R van der Graaf[1] and S Brandenburg[1]

[1] KVI-Center for Advanced Radiation Technology, University of Groningen, Zernikelaan 25, 9747AA Groningen, The Netherlands
[2] Department of Radiation Oncology, University of Groningen, University Medical Center Groningen, PO Box 30001, 9700 RB Groningen, The Netherlands
[3] Department of Electronics and Information Systems, MEDISIP, Ghent University-iMinds Medical IT-IBiTech, De Pintelaan 185 Block B, B-9000 Ghent, Belgium
[4] Helmholtz-Zentrum Dresden—Rossendorf, Institute of Radiation Physics, PF 510119, 01314 Dresden, Germany
[5] Author to whom any correspondence should be addressed.

E-mail: p.g.dendooven@rug.nl

Keywords: proton therapy, positron emission tomography, nitrogen-12, range verification

RECEIVED
13 February 2019

REVISED
3 May 2019

ACCEPTED FOR PUBLICATION
22 May 2019

PUBLISHED
21 June 2019

Abstract

Because of strong indications of multiple counting by the multi-channel scaler (MCS) during most of the experiments described in Dendooven *et al* (2015 *Phys. Med. Biol.* **60** 8923–47), the production of short-lived positron emitters in the stopping of 55 MeV protons in water, carbon, phosphorus and calcium was remeasured. The new results are reported here. With proper single counting of the MCS, the new production rates are 1.1 to 2.9 times smaller than reported in Dendooven *et al* (2015 *Phys. Med. Biol.* **60** 8923–47). The omission of the conversion from MCS time bin to time unit in the previous data analysis was corrected, leading to an increase of the production rate by a factor of 2.5 or 10 for some nuclides. The most copiously produced short-lived nuclides and their production rates relative to the relevant long-lived nuclides are: ^{12}N ($T_{1/2} = 11$ ms) on carbon (5.3% of ^{11}C), ^{29}P ($T_{1/2} = 4.1$ s) on phosphorus (23% of ^{30}P) and ^{38m}K ($T_{1/2} = 0.92$ s) on calcium (173% of ^{38g}K). The number of decays integrated from the start of an irradiation as a function of time during the irradiation of PMMA and 4 tissue materials has been determined. For (carbon-rich) adipose tissue, ^{12}N dominates up to 70 s. On bone tissue, ^{38m}K dominates the beam-on PET counts from 0.2–0.7 s until about 80–110 s. Considering nuclides created on phosphorus and calcium, the short-lived ones provide 8 times more decays than the long-lived ones during a 70 s irradiation. Bone tissue will thus be much better visible in beam-on PET compared to PET imaging after an irradiation. From the estimated number of ^{12}N PET counts, we conclude that, for any tissue, except carbon-poor ones, ^{12}N PET imaging potentially provides equal quality proton range information as prompt gamma imaging with an optimized knife-edge slit camera.

1. Introduction

In the experiments described in 'Short-lived positron emitters in beam-on PET imaging during proton therapy' (Dendooven *et al* 2015), a multi-channel scaler (MCS) registered detector counts versus time, i.e. time spectra. The production of positron emitters follows from the analysis of different half-life components in the beam-off time spectra. Recently, a technical issue was observed related to the MCS: if certain adjustable acquisition parameters are not compatible with signal output/input impedances, the MCS is triggering multiple times on each input signal. As a result, every detector count is registered multiple times and the production deduced is an equal factor too large. After realising this issue, the fact that most reduced χ^2 values of the fits in Dendooven *et al* (2015) are close to 2 suggested that the MCS had been more or less double counting (a doubling of the values of Poisson-distributed data results in a doubling of the χ^2 value of a least-squares fit). The raw data from the experiments described in Dendooven *et al* (2015) do not allow to establish whether this was the case for all

© 2019 Institute of Physics and Engineering in Medicine

experiments, nor whether the double counting was exact or approximate (with e.g. some detector counts being counted once or three times). In order to investigate the above issue, we performed the experiments again and report here on the results.

While analysing the new data, it was noticed that the conversion from MCS time bin to time unit was omitted in the analysis for Dendooven *et al* (2015). Implementation of this conversion in the analysis of Dendooven *et al* (2015) leads to a 10 times lower upper limit for the production of ^{9}C, a 10 times higher production of ^{8}B, ^{38g}K, ^{38m}K and ^{37}K and a 2.5 times higher production of ^{29}P, ^{30}P and ^{30}S. For the other nuclides, the half-life analysis was done using an MCS time bin of either 1 s or 1 ms, for which the conversion to time unit has no impact on the calculation of the production rate. This conversion was implemented in the analysis of the new experiments presented here.

By using a more realistic production profile in the target, a better estimate of the ^{12}N positron escape from the target has been implemented.

The organization of this corrigendum follows that of the original paper Dendooven *et al* (2015) with only changes with respect to that paper being discussed in detail.

2. Materials and methods

In order to be relevant for range verification, the production of positron emitters has to be significant at the distal edge of an irradiation. We therefore measured the integral production of short-lived positron emitters for a relatively low-energy proton beam, 55 MeV, in carbon, oxygen, phosphorus and calcium. The proton beam is pulsed: it is delivered as a succession of beam-on and beam-off periods. Compared to Dendooven *et al* (2015), mostly shorter beam-on periods are chosen in order to favour shorter-lived nuclides over longer-lived ones. Different nuclides are identified based on the half-life analysis of the 511 keV positron annihilation photon time spectra during the beam-off period, see section 2.3 in Dendooven *et al* (2015). The parameters A_0 resulting from the fits represent the nuclide activities per MCS time bin at the beginning of the beam-off period. In the formalism in section 2.3 in Dendooven *et al* (2015), A_0 represents the nuclide activity per time unit; second and millisecond are used in both Dendooven *et al* (2015) and present work. The required conversion from MCS time bin to time unit was omitted in Dendooven *et al* (2015) but is implemented in the present work.

The experiments were performed at the irradiation facility of the AGOR cyclotron at KVI-Center for Advanced Radiation Technology (KVI-CART), University of Groningen. The target properties are given in table 1. The 511 keV annihilation photons were detected by a 51 mm diameter and 51 mm thick NaI(Tl) detector (Scionix Model 51B51/2M). The detector was installed with its axis perpendicular to the beam direction and the centre of its front face at 25 cm from the Bragg peak location. The full energy peak efficiency at 511 keV was measured to be $1.10 \pm 0.01[1\sigma\,\text{statistical}] \pm 0.03[\text{systematic}] \times 10^{-3}$ using a calibrated ^{22}Na source; the statistical uncertainty is deduced from the number of counts in the 511 keV full energy peak, the systematic uncertainty is equal to the source calibration accuracy of 3%. As the target to detector distance is much larger than the proton range, the detector efficiency does not significantly depend on the geometric distribution of the positron annihilation locations and thus does not depend on the target shape. The 511 keV photons were selected using a single channel analyser (SCA) whose output pulses were processed by the MCS. The fraction of the full energy peak inside the SCA energy window was determined to be 0.898.

As a 50 mm thick graphite target was used in the present measurements and a 25 mm thick target in Dendooven *et al* (2015), the correction for escaping positrons needs to be recalculated. However, this is only needed for positron emitters with positron end-point energies sufficiently large such that the escape of positrons is significant. This is the case for ^{12}N and ^{8}B. For the uniform ^{12}N and ^{8}B production profiles in the target as used in Dendooven *et al* (2015), the positron escape fractions become 40% for ^{12}N and 34% for ^{8}B. Since the publication of Dendooven *et al* (2015), we became aware of the experimental data on the ^{12}N production cross section by Rimmer and Fisher (1967) and implemented this information in the simulations presented by Buitenhuis *et al* (2017). For a ^{12}N production profile similar as shown in figure 2 of Buitenhuis *et al* (2017), but for 55 MeV protons, 40% of ^{12}N positrons escape the target. As this is the same value as for the uniform production profile, assuming a different production profile does not influence the production rate deduced from the measurement. The relative systematic uncertainty on the fraction of escaping positrons for the setup considered is estimated to be 10%.

3. Results

3.1. Measured production of positron emitters

In this section, the results of the new measurements are summarized and the differences with the previous results highlighted. Nuclides for which an upper limit was given in Dendooven *et al* (2015) were not remeasured and are thus not included here. In Dendooven *et al* (2015), the production of ^{14}O ($T_{1/2} = 70.6$ s) on ^{16}O was

Table 1. Target properties.

Target	Target thickness (g cm^{-2})	Target form	Range 55 MeV protons[a] (g cm^{-2})
Graphite	8.6	2 stacked 50 mm square, 25 mm thick	2.97
Water	6	Thin-walled polystyrene cup	2.64
Phosphorus	6.0	Red phosphorus powder in 50 mm diameter, 38 mm high plastic container (density 1.26 g cm^{-3}) beam impinging on the curved side wall of the container	3.50
Calcium	4.5	Calcium granules in 69 mm diameter, 45 mm high plastic container (density 0.65 g cm^{-3}) beam impinging on the curved side wall of the container	3.85

[a] From NIST (2015).

determined from the 2313 keV peak seen in the gamma ray energy spectrum taken during the beam-off periods. As this did not involve the MCS, the previously determined production of ^{14}O does not require correction. In Dendooven *et al* (2015), evidence for a contribution of ^{37}K ($T_{1/2} = 1.22$ s) when irradiating the calcium target was seen. However, the data obtained in the present work do not indicate such a contribution. We conclude that the contribution attributed earlier to ^{37}K is now included in the ^{38m}K contribution.

We here incorporate an extra correction factor compared to Dendooven *et al* (2015): a first order correction for attenuation in the targets calculated as the attenuation from the center to the edge of the target in the direction of the detector. The attenuation of 511 keV photons for the graphite, water, phosphorus and calcium targets is 31%, 25%, 23% and 18%, respectively. The attenuation of the 2313 keV gamma ray from ^{14}O in that experiment was 11% and is taken into account as well. Table 2 presents the updated production values, as well as, per nuclide, the reasons for the difference with Dendooven *et al* (2015). The values in table 2 supersede those from Dendooven *et al* (2015). The production of ^{29}P, ^{30}P and ^{30}S is determined from one time spectrum. The correction factor due to the MCS multiple counting is thus the same for these three nuclides. These correction factors deduced from the new/previous production ratios for ^{29}P, ^{30}P and ^{30}S are 0.45, 0.39 and 0.92. We consider the first two to be compatible given the fact that experiments performed a few years apart are compared. The MCS multiple counting correction factor for ^{30}S is not compatible with those of ^{29}P and ^{30}P. Assuming a correction factor for ^{30}S of ~0.4, the production of ^{30}S in the new experiments is 2.3 times larger than in the old experiment. We do not know the reason for this.

One factor increasing the production of ^{38m}K in the new measurements is that the ^{37}K contribution identified in the old measurements is now incorporated in ^{38m}K. In Dendooven *et al* (2015), the ^{37}K production is 0.25 times that of ^{38m}K, giving a factor of 1.25 in the new/previous ratio. After taking into account the time bin conversion factor and MCS multiple counting factor (determined from the ^{38g}K results), a factor of 1.5 remains. We consider this to be compatible with the 1.25 deduced above.

3.2. Number of beam-on PET decays

The results from table 2 are used to determine the production in some representative tissue materials and PMMA, equivalent to table 5 in Dendooven *et al* (2015). Subsequently, the number of PET decays during an irradiation is calculated, equivalent to figures 7 and 8 in Dendooven *et al* (2015). The former of these figures is not reproduced here as the curves for ^{15}O, ^{11}C and ^{12}N on adipose, skeletal muscle and PMMA scale with roughly the same factor, see table 2. The latter of these figures is reproduced in figure 1 as it differs substantially from the one in Dendooven *et al* (2015).

4. Discussion

4.1. Beam-on PET decays

In carbon-rich, oxygen-poor materials, the number of PET decays from ^{12}N dominates for irradiation times up to 70 s in adipose tissue and 45 s in PMMA. For an irradiation time to deliver a dose of 2 Gy in a volume of 1 l, which typically takes 70 s, the fraction of ^{12}N decays relative to the total (including ^{8}B and ^{10}C) is 35% in adipose and 30% in PMMA. This indicates that in beam-on PET during proton irradiations, the PET image in carbon-rich tissue will be deteriorated due to ^{12}N positron range blurring. In oxygen-rich tissue such as illustrated by skeletal muscle here, the deterioration due to ^{12}N will obviously be less severe: for an irradiation time of 70 s, the ^{12}N decays represent just 5% of the total.

For the two types of bone considered, ^{12}N dominates the beam-on PET counts for only up to 0.7 s in compact bone and 0.2 s in cortical bone. At these times, ^{38m}K becomes dominant until its contribution to beam-on PET is surpassed by ^{15}O at 80 s in compact bone and 110 s in cortical bone. The short-lived nuclides produced

Table 2. Production of positron emitting nuclides per 55 MeV proton stopped in the target, with the statistical uncertainty from the fits of the time spectra. The combined systematic uncertainty due to the efficiency calibration of the NaI(Tl) detector and the determination of the fraction of positrons escaping from the target is given separately. The new/previous ratios due to the correction for attenuation in the target and due to other reasons are given.

Nuclide	Target	Production per proton (±statistical uncertainty)	Systematic uncertainty (%)	New/previous ratio due to	
				Correction for attenuation in target	Other reasons
^{15}O	Water	$5.45 \pm 0.04 \times 10^{-3}$	3	1.33	0.46, MCS multiple counting
^{14}O	Water	$8.2 \pm 0.6 \times 10^{-5}$	20	1.12	1.00 (no new measurement)
^{11}C	Carbon	$8.39 \pm 0.06 \times 10^{-3}$	3	1.45	0.72, MCS multiple counting
^{10}C	Carbon	$2.48 \pm 0.16 \times 10^{-4}$	3	1.45	0.56, MCS multiple counting
^{12}N	Carbon	$4.46 \pm 0.13 \times 10^{-4}$	7	1.45	0.42, MCS multiple counting
^{8}B	Carbon	$5.8 \pm 1.2 \times 10^{-5}$	6	1.45	3.6, factor 10 time bin conversion, factor 0.36 MCS multiple counting,
^{29}P	Phosphorus	$1.62 \pm 0.03 \times 10^{-3}$	4	1.30	1.13, factor 2.5 time bin conversion, factor 0.45 MCS multiple counting
^{30}P	Phosphorus	$6.91 \pm 0.05 \times 10^{-3}$	3	1.30	0.98, factor 2.5 time bin conversion, factor 0.39 MCS multiple counting
^{30}S	Phosphorus	$3.9 \pm 0.4 \times 10^{-4}$	5	1.30	2.3, factor 2.5 time bin conversion, factor ~0.4 MCS multiple counting, factor ~2.3 of unknown origin (see text)
^{38g}K	Calcium	$2.77 \pm 0.03 \times 10^{-3}$	3	1.22	4.0, factor 10 time bin conversion, factor 0.40 MCS multiple counting
^{38m}K	Calcium	$4.78 \pm 0.04 \times 10^{-3}$	8	1.22	6.1, factor 10 time bin conversion, factor 0.40 MCS multiple counting, factor 1.5 contribution previously attributed to ^{37}K (see text)

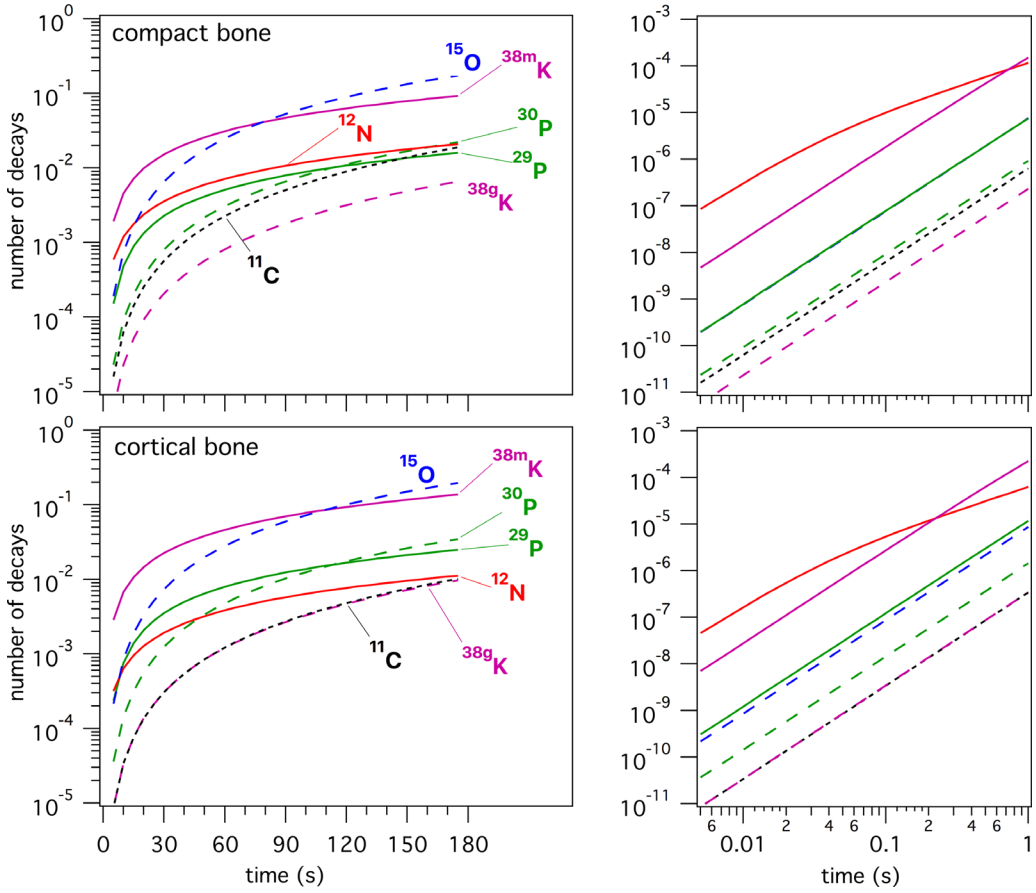

Figure 1. The number of decays of PET nuclides integrated from the start of an irradiation as function of time in the irradiation, for an irradiation with 55 MeV protons and scaled to a beam intensity of 1 proton s^{-1}, for compact bone and cortical bone. Short-lived nuclides are shown with solid lines, long-lived ones with dashed lines. The right column zooms in on the first second of the irradiation.

on phosphorus and calcium, ^{29}P and ^{38m}K, provide a huge increase in PET decays compared to the long-lived nuclides ^{30}P and ^{38g}K. As the production of ^{38m}K is higher than that of ^{38g}K, ^{38m}K will always dominate over ^{38g}K in beam-on PET. For an irradiation time of 70 s for example, ^{38m}K provides 33 times more decays, and thus PET image counts, than ^{38g}K. The observation of ^{29}P in addition to ^{30}P is not as advantageous because the production of ^{29}P is 4 times smaller than that of ^{30}P. Considering nuclides created on phosphorus and calcium, the short-lived ones provide, during a 70 s irradiation, 8 times more decays than the long-lived ones. Bone tissue will thus be far better visible in beam-on PET compared to PET imaging after an irradiation.

4.2. The potential of ^{12}N for prompt PET imaging

We consider the knife-edge slit camera developed by Smeets *et al* (2012) and Perali *et al* (2014) to be the most advanced prompt gamma imaging system presently available. From figures 11 and 12 from Perali *et al* (2014), taking into account the slit resolution, we estimate that the final 55 MeV (2.3 cm) of the proton range yields 3×10^{-6} counts per proton.

The production of ^{12}N in PMMA is 2.4×10^{-4} per 55 MeV proton. Integrated over a time scale of several times the half-life, there will thus be 2.4×10^{-4} ^{12}N decays per proton. Crespo *et al* (2006) calculate PET scanner efficiencies for different scanner geometries, considering spheres of radioactivity of different radius. Attenuation in the phantom is not included. For a radius of activity of 50 mm, a good surrogate for imaging the distal edge of an irradiation, an *in situ* PET scanner with axial length of 32 cm and angular coverage of 270 degrees has a coincidence detection efficiency of about 14 %, thus detecting 3.4×10^{-5} ^{12}N coincidence counts per proton in the absence of attenuation. For comparison with the knife-edge slit camera, attenuation of 511 keV photons in a 15 cm diameter PMMA target as used Perali *et al* (2014) is considered and leads to a reduction of the ^{12}N coincidence counts to 6×10^{-6} per proton.

When considering irradiations in human tissue, the ratio of ^{12}N PET to prompt gamma counts depends on the carbon content of the tissue because ^{12}N is only produced in useful quantities on carbon whereas prompt gamma ray production is rather independent of carbon-to-oxygen ratio (see e.g. Polf *et al* (2009)), with the sum of carbon and oxygen content being rather the same for all soft tissues. For adipose, with a carbon-to-oxygen

ratio of about 2, the ratio of ^{12}N PET to prompt gamma counts will be similar to that of PMMA, i.e. about 2.0. For other tissues, carbon-to-oxygen ratios lie mostly between 1/1.5 and 1/6 (Woodard and White 1986) and the ratio of ^{12}N PET to prompt gamma counts will be from about 1/1.5 to 1/6. Based on number of counts, ^{12}N PET imaging will thus for any tissue except carbon-poor ones provide roughly equal proton range information than prompt gamma imaging using a knife-edge slit camera. However, the number of counts is only one, albeit essential, factor determining the accuracy of range determination. For example, the signal-range correlation is important as well. In this respect, and contrary to most positron emitters, ^{12}N exhibits a sharp production profile (Rimmer and Fisher 1967) similar to that of prompt gamma rays. Also, the neutron background in measured PG profiles, which increases with proton energy and is thus quite substantial for distal edge beams which are most important in range verification, is absent in PET. Dedicated studies to judge the merit of ^{12}N PET in clinically relevant situations are being pursued by the authors.

5. Conclusions

Due to strong indications of an instrumental problem during the experiments described in Dendooven *et al* (2015), the production of short-lived positron emitters in the stopping of 55 MeV protons in water, carbon, phosphorus and calcium was remeasured. An error in the previous data analysis was corrected and a better estimate of the escape of positrons from the target was implemented.

The most copiously produced short-lived nuclides and their production rates relative to the relevant long-lived nuclides are: ^{12}N ($T_{1/2} = 11$ ms) on carbon (5.3% of the ^{11}C production), ^{29}P ($T_{1/2} = 4.1$ s) on phosphorus (23% of the ^{30}P production) and ^{38m}K ($T_{1/2} = 0.92$ s) on calcium (173% of the ^{38g}K production). Using the experimental results, the number of decays of PET nuclides integrated from the start of an irradiation as function of time in the irradiation is calculated for PMMA, adipose, skeletal muscle and compact and cortical bone. The most noticeable result is that for an irradiation in (carbon-rich) adipose tissue, ^{12}N will dominate the beam-on PET image up to 70 s.

On bone tissue, ^{38m}K dominates the beam-on PET counts from 0.2–0.7 s until about 80–110 s. Considering nuclides created on phosphorus and calcium, the short-lived ones provide 8 times more decays than the long-lived ones during a 70 s irradiation. Bone tissue will thus be much better visible in beam-on PET compared to PET imaging after an irradiation.

The ^{12}N positron range image blurring (rms of 18 mm) is similar to the slit resolution (22 mm) of the optimized knife-edge slit camera discussed by Perali *et al* (2014). From the estimated number of ^{12}N PET counts, we conclude that, for any tissue except carbon-poor ones, ^{12}N PET imaging has the potential to provide roughly equal proton range information compared to prompt gamma imaging with an optimized knife-edge slit camera.

ORCID iDs

P Dendooven https://orcid.org/0000-0003-1859-1315
F Fiedler https://orcid.org/0000-0002-2352-2042

References

Buitenhuis H J T, Diblen F, Brzezinski K W, Brandenburg S and Dendooven P 2017 Beam-on imaging of short-lived positron emitters during proton therapy *Phys. Med. Biol.* **62** 4654–72
Crespo P, Shakirin G and Enghardt W 2006 On the detector arrangement for in-beam PET for hadron therapy monitoring *Phys. Med. Biol.* **51** 2143–63
Dendooven P *et al* 2015 Short-lived positron emitters in beam-on PET imaging during proton therapy *Phys. Med. Biol.* **60** 8923–47
NIST 2015 (physics.nist.gov/PhysRefData/Star/Text/PSTAR.html)
Perali I *et al* 2014 Prompt gamma imaging of proton pencil beams at clinical dose rate *Phys. Med. Biol.* **59** 5849–71
Polf J C, Peterson S, Ciangaru G, Gillin M and Beddar S 2009 Prompt gamma-ray emission from biological tissues during proton irradiation: a preliminary study *Phys. Med. Biol.* **54** 731–43
Rimmer E M and Fisher P S 1967 Resonances in the (p,n) reaction on ^{12}C *Nucl. Phys.* A **108** 561–6
Smeets J *et al* 2012 Prompt gamma imaging with a slit camera for real-time range control in proton therapy *Phys. Med. Biol.* **57** 3371–405
Woodard H Q and White D R 1986 The composition of body tissues *Br. J. Radiol.* **59** 1209–18